Biophysical Journal, Volume *111*

Supplemental Information

Mechanical Criterion for the Rupture of a Cell Membrane under Compression

David Gonzalez-Rodriguez, Lionel Guillou, François Cornat, Julie Lafaurie-Janvore, Avin Babataheri, Emmanuel de Langre, Abdul I. Barakat, and Julien Husson

Mechanical criterion for the rupture of a cell membrane under compression

Supplementary Material

D. Gonzalez-Rodriguez*, L. Guillou*, F. Cornat, J. Lafaurie-Janvore, A. Babataheri, E. de Langre, A. I. Barakat, and J.Husson.[1]

* equal contribution

[1]to whom correspondence should be addressed, julien.husson@ladhyx.polytechnique.fr

Supplementary Text

Analytical model relating the displacement of the microindenter's tip to the vertical force it exerts on the cell. We model the microindenter as an inextensible, linear elastic cantilever beam of length l and bending modulus B (Fig. S1A). The tip of the cantilever is attached to a spherical bead of radius R (alternatively, in some of the experiments, the tip is cut and forms a flat punch parallel to the cell surface). The upper end of the cantilever is clamped so as to control its position and prevent rotation. The microindenter is held tilted, initially forming an angle α with the horizontal plane of the sample. During indentation, the position of the upper end is lowered at constant speed, along a straight trajectory that forms an angle of attack β with the vertical direction. We denote the vertical and horizontal displacements imposed to the upper end as δ and λ, respectively. The motion of the upper end induces a vertical indentation of the cell, Δz; moreover, the microindenter's tip glides horizontally by a distance Δx. The cell exerts reaction forces on the bead in the horizontal and vertical directions, denoted H and V. After indentation, the beam adopts a deformed shape described by $\theta(s)$, where θ is the local angle of the beam axis with the horizontal direction and s is the curvilinear coordinate (Fig. S1A). The function $\theta(s)$ can be obtained by imposing equilibrium of torques acting on the cantilever's bead:

$$-Hz - Vx = B\frac{\mathrm{d}\theta}{\mathrm{d}s}\,. \tag{S1}$$

Hereafter we make use of nondimensional variables, denoted by a hat (^). The unit length and force for nondimensionalization are defined based on the microindenter's length, l, and stiffness, $k_\mathrm{m} \equiv B / l^2$. By expressing (x,z) in terms of (s,θ), Eq. (S1) yields an integral equation for $\theta(s)$:

$$\pm\frac{1}{\sqrt{2\hat{F}}}\int_{\theta_0}^{\theta}\frac{\mathrm{d}\theta}{\sqrt{\cos(\theta_F-\theta)-\cos(\theta_F-\theta_0)}} = s\,, \tag{S2}$$

where $F = \sqrt{H^2+V^2}$ is the magnitude of the reaction force and $\hat{F} = F/(k_\mathrm{m} l)$ is the corresponding nondimensional variable. $\theta_F = \mathrm{atan}(V/H)$ is the angle of the reaction force with the vertical, the direction of which must be determined. θ_0 is the inclination of the cantilever at its junction with the tip (Fig. S1A). In Eq. (S2), we will keep the positive sign in front of the integral, which corresponds to a deformed shape where $\mathrm{d}\theta/\mathrm{d}s > 0$, consistent with the experimental curvature of the microindenter. Assuming small deformations, i.e., assuming $\hat{F} = F/(k_\mathrm{m} l) \ll 1$, from Eq. (S2) we can obtain an asymptotic expansion for θ near s=0 in powers of $\hat{F}$:

$$\theta = \theta_0 + \frac{\hat{F}\sin(\theta_F-\theta_0)}{2}\hat{s}^2 - \frac{\hat{F}^2\sin(2\theta_F-2\theta_0)}{48}\hat{s}^4 + O\left(\hat{F}^3\right). \tag{S3}$$

The three unknowns in Eq. (S3), $\hat{F}$, θ_F, and θ_0, are determined by the following three boundary conditions, reflecting the proscribed upper end rotation and the beam's inextensibility:

$$\theta(\hat{s} = 1) = \alpha \,, \tag{S4}$$

$$\int_0^1 \cos\theta \, d\hat{s} = \cos\alpha + \hat{\lambda} + \Delta\hat{x} \,, \tag{S5}$$

$$\int_0^1 \sin\theta \, d\hat{s} = \sin\alpha - \hat{\delta} + \Delta\hat{z} \,. \tag{S6}$$

We recall that a hat (^) indicates a nondimensional variable. In Eqs. (S4-S6), these variables are nondimensional lengths, obtained by dividing the corresponding dimensional variable by the microindenter's length, *l*.

As discussed in the main text, we propose a simple material characterization of the cell with two different regimes. At moderate indentation, $\Delta z \leq \Delta z_{\text{cutoff}}$, the cell is assumed to behave as a non-adhesive homogeneous isotropic linear elastic solid. The value of Δz_{cutoff} corresponds to the limit of validity of the linear elastic regime, which is experimentally estimated to be on the order of $\Delta z_{\text{cutoff}} \approx 0.3$ μm (see discussion in the Results section of the main text). Beyond the linear elastic regime, the cell continues to deform up to a maximum indentation, $\Delta z = \Delta z_{\max}$, at which point it becomes infinitely rigid when compared to the microindenter. This is the onset of the regime that we term "strong indentation". Indeed, the cell will appear progressively stiffer as the indentation becomes larger compared to the sample thickness (Ref. 14 in main text), saturating at indentations of ~60% of the cell height, where the cell becomes nearly infinitely rigid (Refs. 13, 22 in main text).

We first describe the regime of moderate indentation. Here, the Hertz model can be applied and the cell's vertical reaction force written as $V = k_{\text{cell}}(\Delta z)^{3/2}$, where $k_{\text{cell}} = \frac{4}{3}E^*\sqrt{R}$ and $E^* = \frac{E}{(1-\nu^2)}$, with E and ν being the Young's modulus and Poisson's ratio of the cell (4). As discussed in the Results section of the main text, we experimentally observe that friction between the microindenter and the cell is negligibly small. For this reason, when describing the moderate indentation regime, we can neglect the horizontal component of the reaction force, i.e., assume H=0 and θ_F=π/2. With these assumptions, Eqs. (S3-S6) yield to leading order

$$\Delta x_{\text{eff}} \equiv \Delta x + \lambda = \frac{2\sin 2\alpha}{9}\frac{E^*\sqrt{R}}{k_{\text{m}}}\delta^{3/2}. \tag{S7}$$

Next, we describe the regime of strong indentation, which starts once the maximum indentation is attained ($\Delta z = \Delta z_{\max}$). In this regime we consider that the cell behaves as a rigid body with Coulomb friction, i.e., we assume $\Delta z = \Delta z_{\max} = \text{constant}$ and $|H/V| = \mu$, the dynamic friction coefficient between the microindenter and the cell membrane. We note that, in contrast with our hypothesis to study the moderate indentation regime (Eq. S7), in the following we do not assume a priori that friction can be neglected. The reason is that the equations of the strong indentation regime are used to estimate a value of μ, by comparison to experimental data (Fig. 3B in the main text). With these assumptions, Eqs. (S3-S6) yield, to leading order:

$$\Delta x_{\text{eff}} \equiv \Delta x + \lambda = \tan\alpha\,(\delta - D_{\text{lin}}) \,, \tag{S8}$$

where Δx_{eff} is a newly defined variable representing the elongation of the microindenter's horizontal projection, and D_{lin} is a constant (Fig. S1B). We also obtain that

$$\Delta x = \delta(\tan\alpha - \tan\beta) = \frac{V}{k_m}(\tan\alpha - \tan\beta)(\cos^2\alpha + \text{sign}(\beta - \alpha)\mu\sin\alpha\cos\alpha) \,. \tag{S9}$$

Eq. (S9) can be applied to membrane rupture conditions, denoted by an asterisk (*): $\Delta x = \Delta x^*$, $V = V^* = \sigma^* S_{\text{contact}}$. By measuring Δx^* for different values of the angle of attack, β, Eq. (S9) enables the

calculation of the friction coefficient μ. If we consider the case where the imposed displacement of the upper end is vertical (β=0) and assuming negligible friction between the microindenter and the cell (μ≈0, see discussion in the main text), Eq. (S9) simply reduces to

$$V = 2\,k_{\mathrm{m}}\Delta x\,/\,\sin(2\alpha). \tag{S10}$$

Moderate indentations provide an estimate of the cell's apparent Young's modulus. The normal force applied by the microindenter onto the cell can be deduced from the measurement of the horizontal displacement of the microindenter's tip. By assuming that the contact between the microindenter and the cell is described by Hertz's model (Ref. 39 in main text), we can use tilted microindentation to estimate the local apparent Young's modulus of the cell, E^*. To this end, we record the horizontal displacement of the microindenter's tip, Δx, as a function of the imposed vertical displacement of its upper end, δ. We obtain an indentation curve of the form represented in Fig. S1B.

We fit Eq. (S7) to each curve in order to find, for each tilted microindentation, the value of E* that best fits the relation between the measured horizontal displacement of the microindenter's tip, Δx, and the corresponding vertical displacement of the upper end of the microindenter, δ (Fig. S3). We emphasize that δ is the vertical displacement of the upper end of the microindenter, and not the actual vertical indentation of the cell, Δz. Both magnitudes are similar for moderate indentations, for which the indenter deforms little. However, once the indenter starts to significantly deform, δ continues to increase, whereas Δz attains a maximum value, as discussed in the main text.

The fit is performed from the beginning of the indentation, $\delta = 0$, up to a cutoff value, $\delta = \delta_{\mathrm{cutoff}}$, which should correspond to the limit of validity of Hertz's contact theory, estimated at $\delta/h \geq \Delta z/h \approx 0.3$ (see Fig. S4). Using this approach, we are able to resolve regional differences in apparent Young's modulus of endothelial cells and find that it varies from $E^* = 5.4 \pm 0.8$ kPa on the nucleus to $E^* = 8.0 \pm 1.0$ kPa on the perinuclear region and $E^* = 17.3 \pm 2.7$ kPa on the cytoplasm (the tendency is clear, although only the difference between the nucleus and the cytoplasm is statistically significant in our data). For the nucleus and the perinuclear region, the apparent Young's modulus is insensitive to the choice of δ_{cutoff}, even when the fit is continued beyond the Hertz regime. In contrast, we do find variations up to ~50% for experiments done on the cytoplasm (Fig. S3A). This is presumably due to the fact that the deformation inside the cell, which scales with δ/h, where h is the height of the sample, cannot be neglected for indentations performed on the cytoplasm, for which $h \sim 1\ \mu m$, when δ exceeds a few hundred nanometers. Therefore, when tilted microindentation is performed on the cytoplasm, it is best to limit the data range to $\delta \leq \delta_{\mathrm{cutoff}} = 0.3$ μm, as was done in Fig. S3B.

Overall, we measure Young's moduli that are consistently on the order of the kPa, in agreement with typical values previously reported for endothelial cells (Ref. 24 in main text).

Supplementary Figures

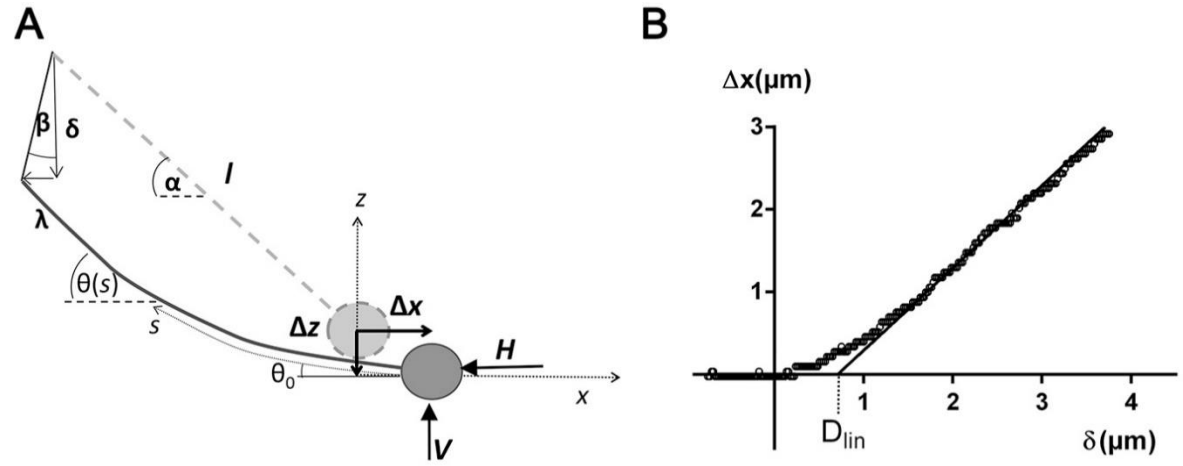

Figure S1. Relationship between imposed vertical displacement and horizontal displacement of the microindenter's tip. *(A)* Geometric parameters defining the deformation of the microindenter. *(B)* Example of the measured horizontal displacement of the microindenter's tip, Δx, as a function of the imposed vertical displacement of the upper end of the microindenter, δ.

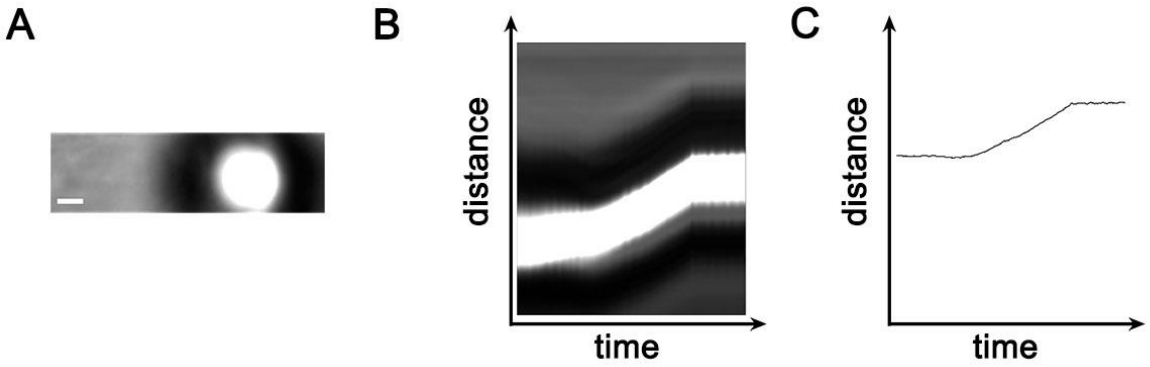

Figure S2. Analysis of tilted microindentation used to characterize the moderate indentation regime. *(A)* Image extracted from Movie S2. *(B)* Kymogram obtained after importing Movie S1 in ImageJ, normalizing and smoothing the images, and then defining a line along the horizontal bead trajectory when sliding on the surface of the cell. The kymogram represents this line at each frame, forming a distance–time graph coded in gray scale intensity. *(C)* The kymogram is then thresholded in order to select the dark rim of the bead. The image is binarized according to this threshold, resulting in the distance-time graph shown. The resulting (position, frame number) coordinates of the edge of the binary are then stored in a text file.

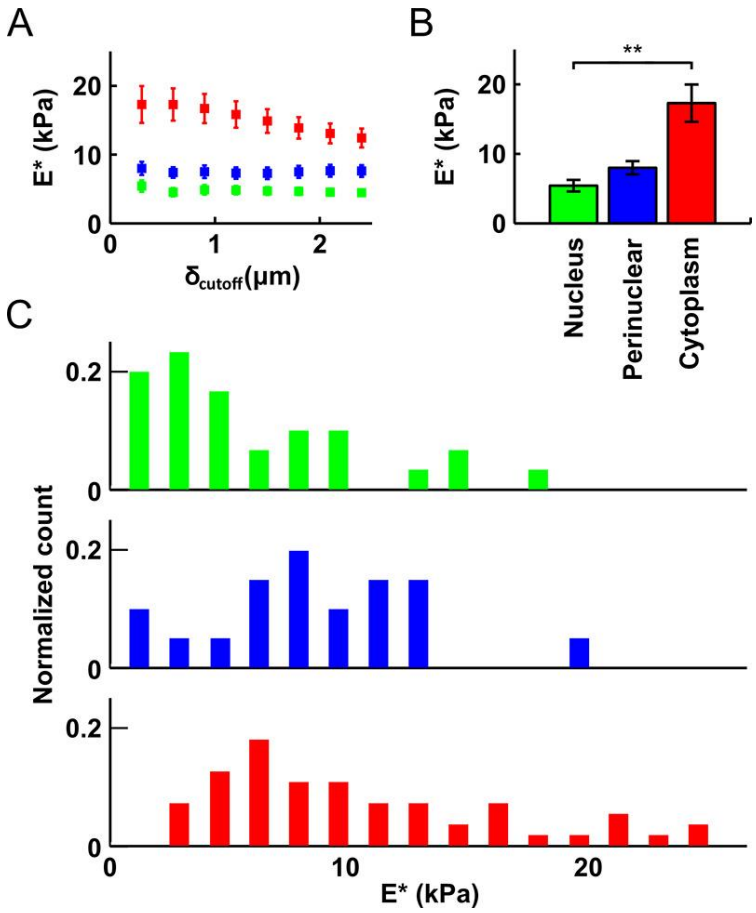

Figure S3. Tilted microindentation provides an estimate of the cell's apparent Young's modulus E*. To this end, we employ Eq. (S7) to find the value of E* that best describes the relation between the measured horizontal displacement of the microindenter's tip Δx and the corresponding vertical displacement of the upper end of the microindenter δ. Tilted microindentation was performed on the cytoplasm (red), the perinuclear region (blue), and the nucleus (green). *(A)* Estimated Young's modulus E* as the cutoff point for the data fit, $\delta = \delta_{\mathrm{cutoff}}$, is varied from 0.3 μm to 2.4 μm. *(B)* For $\delta_{\mathrm{cutoff}} = 0.3$ μm, the apparent Young's modulus varies from $E^* = 5.4 \pm 0.8$ kPa on the nucleus to $E^* = 8.0 \pm 1.0$ kPa on the perinuclear region and $E^* = 17.3 \pm 2.7$ kPa on the cytoplasm (**p<0.01). *(C)* Distribution of the apparent Young's modulus E* across the three cell regions on which tilted microindentation was performed. Normalized count indicates the share of microindentations that led to a given value of the apparent Young's modulus.

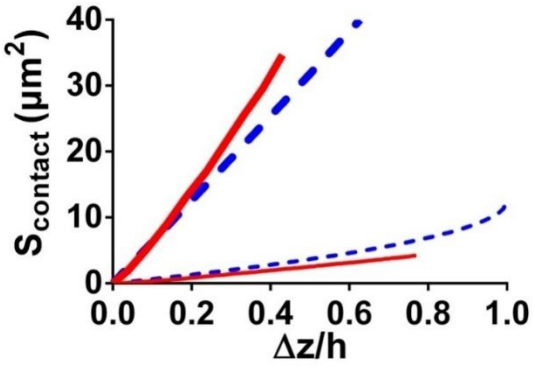

Figure S4. Numerical simulations (solid lines) of the relationship between the contact area, S_{contact}, and the indentation normalized by the cell thickness, $\Delta z/h$. The cell is modeled as a hyperelastic medium of finite thickness, h. The dashed lines correspond to the modified Hertz model, $S_{contact} = 2\pi R\,\Delta z$. The thin lines correspond to $R/h = 1$ and the thick lines to $R/h = 10$.

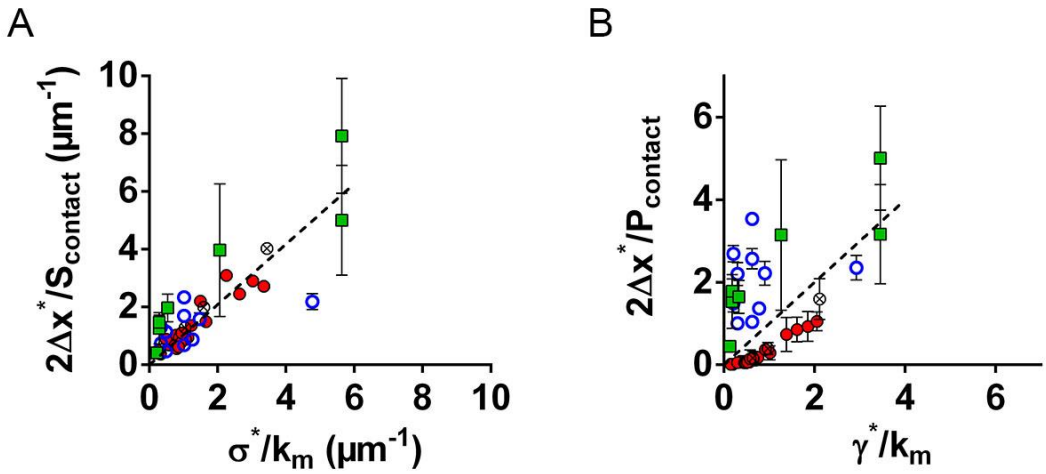

Figure S5. Comparison between the goodness of fit of two rupture criteria, based on either a critical stress (in plot A) or a critical tension (in plot B). Data from Fig. 2D in the main text are used. The displacement of the microindenter's tip at membrane rupture, Δx^*, is normalized by either the area, $S_{contact,}$, (in plot A) or by the perimeter, $P_{contact}$, (in plot B) of the contact surface between the microindenter's tip and the cell. This normalized displacement is represented as a function of the inverse of the stiffness, k_m, normalized by either a best-fit critical stress, σ^*=12.4 kPa, (in panel A) or by a best-fit critical tension, γ^* = 7.6 nN/μm, (in panel B). Different geometries of the microindenter's tip are used: spherical tip (full circles, N = 133 cells), rectangular flat tip (empty squares, N = 41 cells), circular flat tip (empty circles, N = 134 cells). The encircled crosses correspond to spherical-tip microindentation measurements upon cytochalasin-D treatment. Error bars represent standard error of the mean. For all cases, $\alpha = 45°$. The dashed line is a linear fit of all data. A dashed line of slope 1 and coefficient of determination of 1 would indicate that the proposed normalization yields a perfect collapse of all data. *(A)* The best linear fit obtained with a critical stress criterion, with $\sigma^* = 12.4$ kPa, has a slope of 1.04±0.06 and a coefficient of determination R^2=0.7. *(B)* The best linear fit obtained with a critical tension criterion, γ^* = 7.6 nN/μm, has a slope of 1.0±0.1 but a markedly lower value of R^2=0.25.

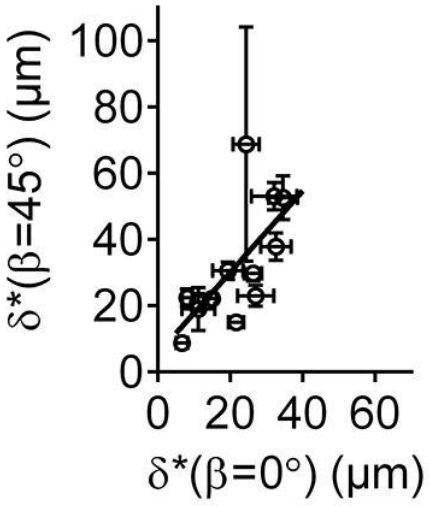

Figure S6. Cell membrane rupture is obtained for the same vertical displacement of the upper end of the microindenter, δ*, for angles of attack β=0 degrees and β=45 degrees. Each circle represents between 4 and 7 cells with 13 different microindenters of spherical tips. Error bars are standard error of the mean. The straight line is a linear fit of the data: $\delta^*(\beta = 45°) = (1.2 \pm 0.4)\delta^*(\beta = 0°) + (6 \pm 9)\ \mu m$.

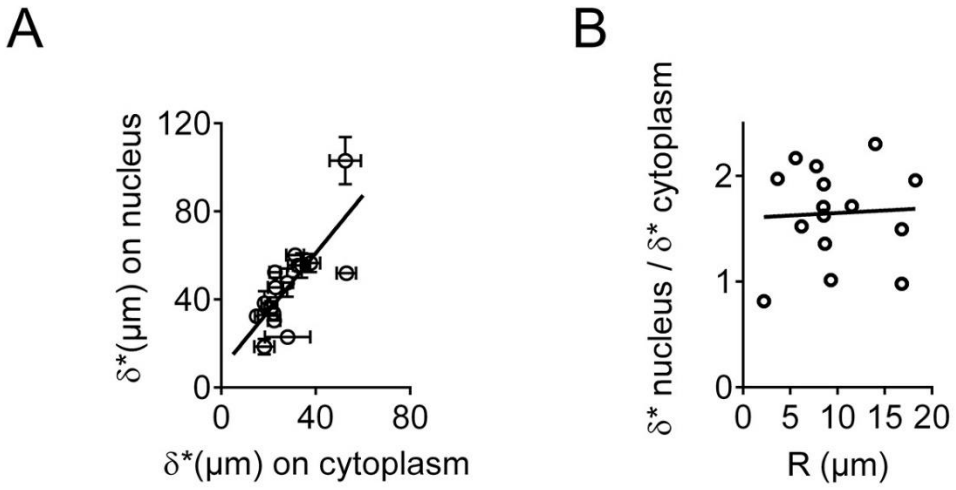

Figure S7. *(A)* Cell membrane rupture occurs at a comparable but slightly larger displacement δ* when compressing a cell on top of the nucleus than when compressing it on top of the thin parts of its cytoplasm. The microindentation is performed at an angle of attack β=45 degrees with 11 microindenters with spherical tips of varying radius *R*. Each circle represents between 4 and 9 cells, error bars are standard errors of the mean. The straight line is a linear fit of the data: $\delta^*_{nucleus} = (1.3 \pm 0.3)\delta^*_{cytoplasm} + (9 \pm 9)\ \mu m$. *(B)* The ratio $\delta^*_{nucleus}/\delta^*_{cytoplasm}$ is independent of the radius of the microindenter, R. The data are the same as in (A) but plotted against *R*. The straight line is a linear fit to the data, $\delta^*_{nucleus}/\delta^*_{cytoplasm} = (1.6 \pm 0.3) + (0.005 \pm 0.025)R$.

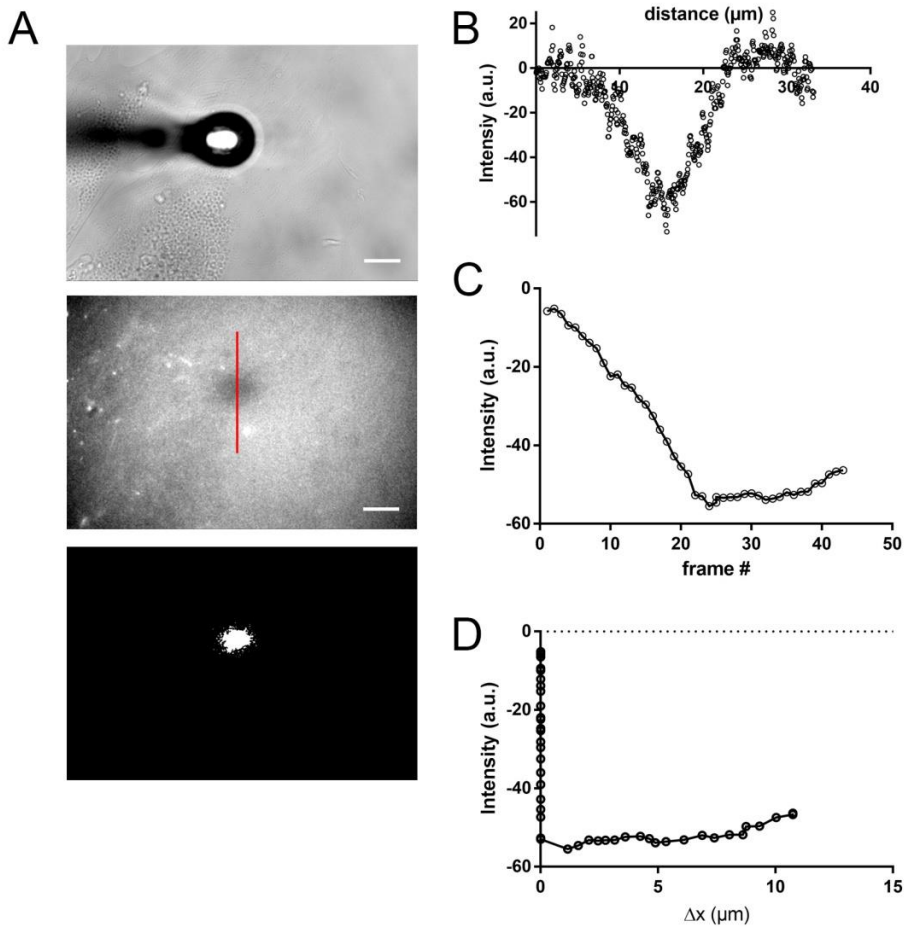

Figure S8. Experimental determination of the bead-cell contact surface area. *(A)* Snapshot under bright field (top) and fluorescence (middle) illumination of a spherical microindenter pushed against the surface of an endothelial cell. A dark spot smaller than the indenting sphere is detected in fluorescence (middle). Upon automatic thresholding using ImageJ software, the measured area of the dark sport is considered a good indication of the surface contact area. *(B)* Intensity profile along the red line plotted in the fluorescence image in *A*, showing the intensity drop under the microindenter. *(C)* Average fluorescence intensity measured under the indenter corresponding to Movie S7. The background intensity has been subtracted from each frame. The intensity drops monotonically upon compression of the cell, until a plateau of constant fluorescence intensity is reached, corresponding to a dark spot that is constant in shape and intensity. *(D)* Average fluorescence intensity measured under the indenter for the experiment in Movie S7 and plotted against the sliding distance Δx of the microindenter's bead. A constant intensity is reached as soon as the sliding of the bead is initiated.

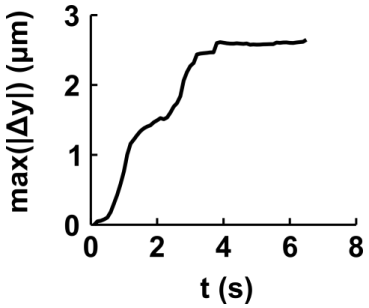

Figure S9. The radial displacement inside the cell during tilted microindentation is estimated by tracking the displacement of mitochondria. We report here the average of the top 10 values of radial displacement Δy of mitochondria over time during tilted microindentation. To obtain those maximum values, we tracked 1421 points at each frame, as shown in Movie S3.

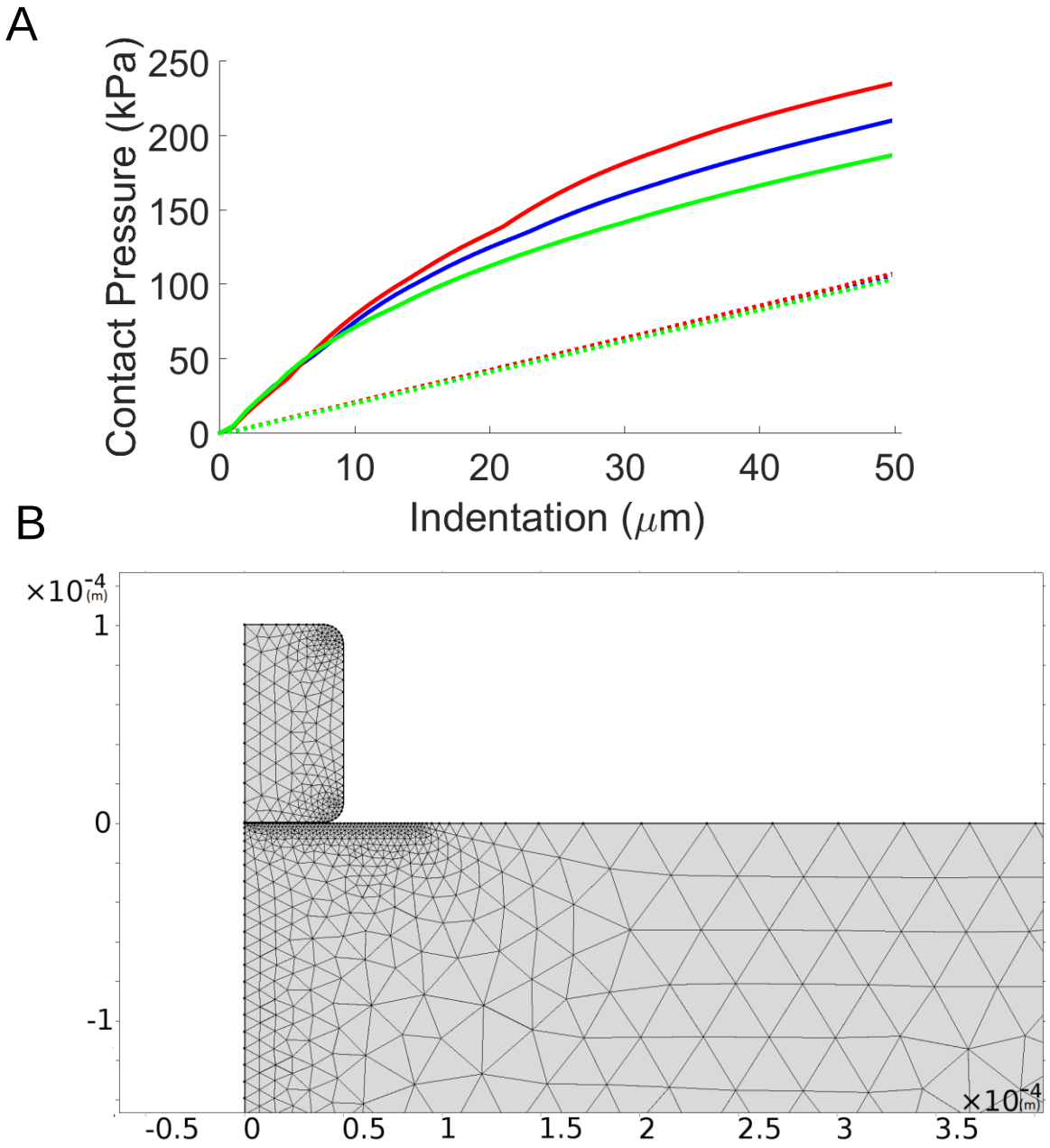

Figure S10. Concentration of stress under a cylindrical indenter (flat punch). *(A)* Maximal and average contact pressure as a function of the penetration depth of a cylindrical indenter into the artery wall. Full curves correspond to maximal pressures and dashed curves to average pressures, whereas the different colors correspond to different radii of curvature of the edge of the indenter. The colors blue, red and green correspond respectively to a fillet of 5, 10 and 20 µm. Overall, the stress concentration factor, defined as the ratio between the maximum and the average contact pressure, can roughly be approximated to be on the order of 3. *(B)* Mesh used in the numerical simulations

Supplementary Movie Legends

Movie S1. Tilted microindentation to characterize cell membrane rupture.

Tilted microindentation of a bovine aortic endothelial cell used to characterize cell membrane rupture. Brightfield illumination is shown in the upper left panel, fluorescence imaging of propidium iodide is shown in the upper right panel, fluorescence imaging of fluo-4 is shown in the lower left panel, and merged channels are shown in the lower right panel. The three channels are obtained using a 100x objective at an acquisition rate of 0.5 frames per second. The movie plays at 10 frames per second, so the movie is accelerated 5 times. Scale bar is 10 μm. Upon membrane rupture, both propidium iodide and extracellular calcium enter the cell cytoplasm, which leads to a rapid increase in the fluorescence levels. It is noted that the two agents exhibit different diffusion rates in the cell cytoplasm.

Movie S2. Tilted microindentation to characterize the moderate indentation regime.

Tilted microindentation of a bovine aortic endothelial cell used to characterize the moderate indentation regime. We use brightfield illumination, focus the microscope 3.5 μm below the basal plane of the cell's basal plane, and define a region of interest to limit computer memory usage. The acquisition is performed at 100 frames per second and 5 ms exposure time. Scale bar is 2 μm. The base of the probe is translated at 2 μm/s. We measured the position of the edge of the bead as a function of time as described in Figure S2.

Movie S3 Particle Image Velocimetry using mitochondria during indentation.

Tilted microindentation of a bovine aortic endothelial cell with fluorescently labeled mitochondria. On the left side, the fluorescent images are obtained using a 100x objective at an acquisition rate of 10 frames per second. The movie plays at 7 frames per second, so the movie is slowed 1.4 times compared to the experiment. Scale bar is 5 μm. To visualize the mitochondria, BAECs were incubated before the experiment for 30 min in mitotracker M7510, as detailed in Gonzalez-Rodriguez et al. (ref. 40 in main text). On the right side, we used the CRToolbox developed and made freely available online by Julien Diener at https://sites.google.com/site/crtoolbox/home to track the displacements of the mitochondria [Diener et al., 2012, Proceedings of the 7th International Biomechanics Conference, Clermont-Ferrand, p. 179]. From there, we used a custom-made Matlab code to visualize the 2D displacements. Circles indicate a virtual particle that is tracked over time. Lines indicate the displacements of said virtual particles.

Movies S4. Simulation of cell indentation in FEBio.

Colormap of the radial deformation under the microindenter for the case $R/h = 1$.The imposed indentation $\Delta z/h$, which lies between 0 and 0.79, increases linearly over the movie's duration. The movie plays at 7 frames per second, corresponding to 7% indentation per second (one frame marks 1% indentation, except for the last three frames in which the indentation steps are slightly smaller).

Movie S5. Simulation of stent deployment.

Displacements are represented at scale 1 and the color represents the von Mises stress in the artery wall. The black lines represent the original position of the artery before indentation.

Movie S6. Fabrication of microindenters with a spherical tip of different size.

A smartphone was placed on a 3D-printed custom-made adapter to record through the oculus of a microforge while forging a microindenter. On the right of each of both panels, a submillimetric glass bead placed on a heating wire is melted and used to form a microbead at the tip of a micropipette (on the left of both panels) previously cut to the desired diameter. The movie is played in real time and demonstrates how beads of various sizes can be formed at the tip of a microindenter.

Movie S7. Experimental determination of the bead-cell contact surface area.

Tilted microindentation of a bovine aortic endothelial cell with a spherical microindenter. Both brightfield (top) and fluorescence (bottom) illumination are used. Upon indentation, a dark spot appears under the tip of the microindenter. This dark spot is indicative of the bead-cell contact area. The acquisition is performed at 1 frame per second. The scale bar represents 10 μm.

Movie S8. The radial displacement inside the cell during tilted microindentation is tracked over time.

This is the same tilted microindentation as in movie S3, but instead of reporting the displacement vectors, we show here the radial displacement over time as a heat map. Dark red corresponds to a radial displacement of 4 μm towards the top of the image, while dark blue corresponds to a radial displacement of 4 μm in the opposite direction. We see a rift where the radial displacement switches direction (i.e. where the color map switches from red to blue), which corresponds to the location where the microindenter's tip has passed.